

**Modulation instability and rogue waves for shear flows with a free surface**Q. Pan,<sup>1,\*</sup> R. H. J. Grimshaw,<sup>2</sup> and K. W. Chow<sup>1</sup><sup>1</sup>*Department of Mechanical Engineering, University of Hong Kong, Pokfulam, Hong Kong*<sup>2</sup>*Department of Mathematics, University College London, London WC1E 6BT, United Kingdom*

(Received 17 May 2019; published 29 August 2019)

We study free surface gravity waves in the presence of a depth-dependent shear current with a nonzero vorticity gradient. The evolution of weakly nonlinear, narrow-band wave packets is governed by a nonlinear Schrödinger equation. When dispersion and nonlinearity are of the same (opposite) signs, modulation instability will be present (absent), and rogue waves represented by breathers can (cannot) occur, respectively. For irrotational flows, rogue waves only occur for sufficiently deep water, or more precisely,  $kh > 1.363$ , where  $k$  is the wave number of the carrier envelope and  $h$  is the water depth. While the irrotational and linear shear current cases have been treated previously, the present study demonstrates the importance of a shear current with a nonzero vorticity gradient. For a concave current, the threshold for modulation instability of a wave packet moving with (or against) the shear current will reduce (or increase) the numerical bound of 1.363, respectively. The opposite will hold for the case of a convex current. The growth rate of a disturbance will also be larger for concave currents in comparison with convex and linear currents. The streamline patterns for the transient case of rogue waves will be illustrated for the simple case of a linear shear current. Shear currents near the sea surface are known to have a profound influence on the dynamics of wind-generated waves, and the present investigation bears on this.

DOI: [10.1103/PhysRevFluids.4.084803](https://doi.org/10.1103/PhysRevFluids.4.084803)**I. INTRODUCTION**

The propagation of slowly varying, narrow-band wave packets on the free surface of a fluid is important both in terms of theoretical hydrodynamics and applications in oceanography, affecting the dynamics of marine vessels and the safety of offshore structures. The competition between dispersion and nonlinearity for water waves also serves as a vivid example for the intriguing physics of fluids and other media. Asymptotic multiple scale perturbation theory typically leads to members of the hierarchy of nonlinear Schrödinger equations as governing models [1,2]. Modulation instabilities arising from the interplay of dispersive and nonlinear effects will cause small disturbances imposed on a plane-wave background to grow exponentially. At moderate to finite amplitude the instability will saturate and eventually an almost periodic motion occurs, commonly called the Fermi-Pasta-Ulam recurrence [3–5]. For water waves, this instability occurs only for sufficiently deep water, namely,  $kh > 1.363$ , with  $k =$  wave number of the carrier envelope, and  $h =$  water depth [1,2].

Nonlinear amplitude equations have been utilized extensively in the studies of water waves, e.g., modeling the effects of topography [6]. To increase the range of validity of these perturbation theories, extensions to the fourth-order terms of the (small) nonlinear parameter have frequently been performed [7,8]. Fourth-order nonlinearities, wind forcing, or other factors may destroy the

---

\*Corresponding author: [upanqing@connect.hku.hk](mailto:upanqing@connect.hku.hk)

symmetry of the most unstable modulation instability “sidebands” of the nonlinear Schrödinger equation and lead to frequency “downshifting” [9,10]. Even at the regime of cubic nonlinearity, resonance can occur between long and short waves for special parameters, and the timescale of interaction may be shorter [11].

Rogue waves have captured the attention of many scientists in fluid mechanics, optics, and plasma through their abrupt and transient growth from an otherwise tranquil background [12–14]. In fluid mechanics, both deterministic and probabilistic approaches have been pursued, but we are concerned with the former aspect in this work. A widely used model is the nonlinear Schrödinger equation. Rogue waves represented by breather solutions are only permitted when dispersion and nonlinearity are of the same sign, i.e., regime with modulation instability. These studies on rogue waves brought attention to the  $kh > 1.363$  constraint, although the numerical value of this limit may be modified due to oblique perturbations or the influence of currents [15,16]. Remarkably, these localized pulses and rogue waves can be detected or measured in a laboratory setting [17,18].

Recently, the connection between modulation instability and rogue waves has been studied intensively. Rogue waves, represented as breathers in the nonlinear Schrödinger and other evolution equations, exist for those parameters where the modulation instability spectrum contains the low-frequency components, also widely known in the literature as baseband instability [19–21]. Numerically, extensive simulations have confirmed that rogue waves can only be excited from a weakly perturbed continuous wave if baseband instability is present.

A significant portion of the literature on water waves is based on the assumption of irrotational flows, but wave-current interaction may exert a nontrivial influence in many applications, both in laboratory and in geophysical settings. In general, the presence of shear flows can play a significant role in oceanic scenarios [22,23].

The literature on small and finite amplitude waves in even a linear shear velocity profile is too numerous for a comprehensive review. Hence only a brief survey is attempted here. Starting from early studies on the geometric shapes of the wave profiles in layered fluids with shear currents [24], recent efforts have touched upon many aspects of fluid dynamics, such as stability, scattering, and particle paths [25,26]. Even apparently simple issues like particle paths actually display surprisingly rich structures. In the long wave regime where the Korteweg–de Vries theory applies, the analysis is slightly simpler and already offers a glimpse of the intriguing issues involved. For instance, pressure inversion can occur where fluids with higher pressure are located above those with a lower pressure [27]. Wave breaking can be investigated too [28].

Here we first review the connection between the nonlinear Schrödinger equation and free surface flows with a linear shear current. Calculations of the induced mean flow and the second harmonic in the presence of a flow with linear shear current (i.e., uniform vorticity) will indeed generate the nonlinear Schrödinger equation as the governing model [29,30]. Before extending the consideration to arbitrary shear profiles (the main purpose of this paper), a remark on the linear theory is in order. In general, any shear current will create a preferred direction, and the mode going with (against) the current will be termed the *forward* (*backward*) mode, respectively, in this paper. In other words, forward (backward) modes refer to downstream (upstream) propagating modes. Critical layers may be present if the shear flow speed matches the phase velocity of the wave within the flow domain. Such singularities may lead to significant energy exchange between the wave and the flow, and will be left for future studies. We only examine modes without any such critical layers here. For the simple case of a linear shear profile without critical level, the modulation instability of the backward mode, i.e., the growth rates of the perturbations, is reduced. However, for the forward mode, these growth rates of the perturbations increase if  $kh$  is small and then subside as  $kh$  increases.

For backward modes (i.e., modes traveling against the current), the propagation of envelope solitary waves of the nonlinear Schrödinger type may exhibit closed streamlines or recirculation regions, which can have significant implications in the dynamics and volume flux [31–33]. The effect of surface tension is ignored here and will be pursued in the future [34].

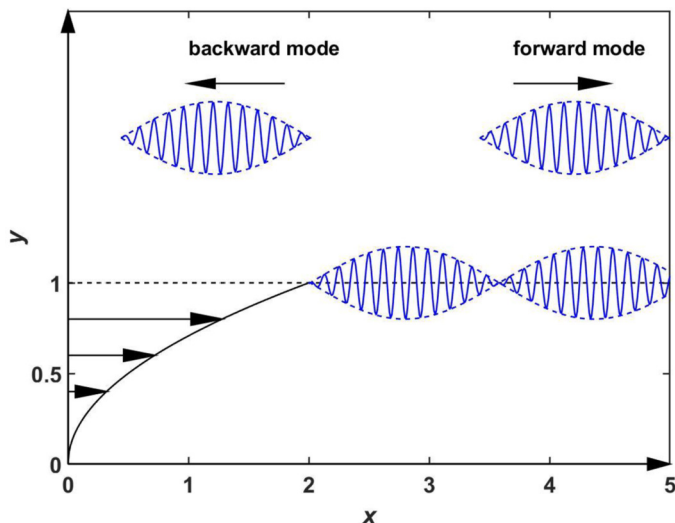


FIG. 1. A schematic view of a wave packet propagating in a shear flow with nonzero vorticity gradient. The upper surface ( $y = 1$ ) is free, but the bottom ( $y = 0$ ) is flat and rigid.

The main goal of this work is to study the existence condition of rogue waves, represented as breathers, on the free surface of a fluid with an otherwise arbitrary shear current profile, through the onset of modulation instability of the nonlinear Schrödinger equation. Although some quite lengthy formulations have been given in the literature, no detailed calculations have apparently been attempted, and hence no interpretation in terms of the possible occurrence of rogue waves has been made. Furthermore, we offer here a preliminary attempt to tackle delicate dynamical issues such as the particle paths. Although streamlines for propagating solitary wave envelopes for a linear shear current have been investigated, no serious discussions on the counterparts for transient motions like rogue waves have been given.

We begin by outlining the theoretical formulation (Sec. II). The results for a linear shear flow and comparisons with the literature are then listed (Sec. III). The main themes of the work, namely, conditions for the presence of rogue waves for convex and concave shear profiles, are presented (Sec. IV), followed by a growth rate analysis (Sec. V). Streamlines of such rogue waves on currents are drawn and elucidated (Sec. VI). Finally, we present the conclusions (Sec. VII).

## II. FORMULATION

### A. Derivation of the nonlinear Schrödinger equation

The objective is to study the evolution of slowly varying, narrow-band wave packets on an arbitrary shear flow with a free surface (at the undisturbed level  $y = 1$  in the nondimensional variable) and a flat rigid bottom ( $y = 0$ ) (Fig. 1). If the shear velocity is a linear function of the vertical coordinate, the irrotational flow assumption still holds for two-dimensional disturbances (but not three-dimensional ones) [25,31–33]. These considerations can be extended to gravity-capillary waves where surface tension is taken into account [34]. Indeed a nonlinear Schrödinger equation type analysis represents a special kind of four-wave interaction involving sidebands. A more general viewpoint can be adopted including disturbances of larger amplitude and other quartet instabilities [35].

The goal here is to extend the investigation to shear current of arbitrary profiles. Although a Lagrangian approach has been used in the literature [36], we find here that the usual Eulerian approach is more convenient. Formulations for wave-packet evolution have been given earlier in

the literature where long expressions involving the shear flows are inevitable [37–39]. The vertical structure of small amplitude disturbance is then described to leading order by a Rayleigh equation. The second harmonic and the induced mean flow are then calculated sequentially. At the third order in an expansion using a small amplitude parameter, a solvability condition will yield the nonlinear Schrödinger equation.

For completeness, a brief description will be outlined here. The vertical velocity ( $v$ ) is first expanded as

$$\begin{aligned} v &= \varepsilon v_1 E + \text{c.c.} + \varepsilon^2 v_{2,2} E^2 + \text{c.c.} + \varepsilon^2 v_{2,1} E + \text{c.c.} + \varepsilon^2 v_{2,0} + \varepsilon^3 v_{3,1} E^3 + \text{c.c.} + \dots, \\ E &= \exp[i(kx - \omega t)], \end{aligned} \quad (1a)$$

where  $\varepsilon$ ,  $k$ ,  $\omega$ , and c.c. stand for the small amplitude parameter, carrier wave number, angular frequency, and complex conjugate, respectively. The horizontal velocity and pressure will have similar asymptotic expansions, except that a basic current shear  $U(y)$  and a hydrostatic pressure background, respectively, will also be needed. The free surface displacement has a similar series representation. Gravity is “nondimensionalized” to unity.

To leading order, the velocity  $v_1$  is given by

$$v_1 = \phi(y)S(X - c_g T, \tau), \quad (1b)$$

where  $S$  is the slowly varying envelope and  $\phi$  is given by the Rayleigh equation

$$\frac{d^2 \phi}{dy^2} - \left[ k^2 + \frac{U''}{U - c} \right] \phi = 0, \quad U = U(y), \quad (1c)$$

$$c = \omega/k = \text{phase speed}, \quad c_g = \text{group velocity},$$

$$X = \varepsilon x, \quad T = \varepsilon t, \quad \xi = \varepsilon(x - c_g t), \quad \tau = \varepsilon^2 t, \quad (1d)$$

being the slow scales. The  $O(\varepsilon)$  or small amplitude regime determines the phase speed through Eqs. (1b) and (1c) and the boundary condition

$$\phi(0) = 0 \quad \text{and} \quad \phi'(1) - \left( \frac{U'(1)}{U(1) - c} + \frac{1}{[U(1) - c]^2} \right) \phi(1) = 0. \quad (1e)$$

Physically the first condition of Eq. (1e) denotes no fluid penetration at a rigid bottom. The second condition combines a usual kinematic condition (particle starts at the free surface and remains there) and a dynamic condition of pressure being constant at the free surface. Numerically an iterative procedure is used. Starting from a trial value of  $c$ , Eq. (1c) is integrated from  $y = 0$  towards  $y = 1$ . This procedure is repeated until the second condition of Eq. (1e) is satisfied by a secant method of determining the root of the equation.

The second-order terms  $v_{2,2}$ ,  $v_{2,1}$ , and  $v_{2,0}$  will be proportional to  $S^2$ ,  $S_X$ , and  $SS^*$  (\* = complex conjugate), respectively. The Fredholm alternative theorem will then be used for the  $\varepsilon^3 \exp[i(kx - \omega t)]$  term for solvability, leading to the nonlinear Schrödinger equation for the evolution of the envelope in a frame of reference moving with the group velocity:

$$iS_\tau + \beta S_{\xi\xi} + \gamma S^2 S^* = 0. \quad (2)$$

The full formulation leading to the derivation of Eq. (2) is given in Appendix B. A plane Stokes wave of amplitude  $S_0$  is given by the solution

$$S = S_0 \exp[i\gamma S_0^2 \tau]. \quad (3)$$

Here without loss of generality  $S_0$  is taken as real-valued. Following widely used convention in the literature, we adopt the Peregrine breather solution of Eq. (2) as a model for a rogue wave [12,14,19,20]:

$$S = S_0 \exp(i\gamma S_0^2 \tau) \left[ \frac{4\beta(1 + 2i\gamma S_0^2 \tau)}{\beta + 2S_0^2 \gamma \xi^2 + 4\beta \gamma^2 S_0^4 \tau^2} - 1 \right]. \quad (4)$$

Different shear flows  $U(y)$  will give distinct values of  $\beta$  and  $\gamma$ . The amplitude of the rogue wave relative to the background ( $S_0$ ) is always three, but in general increasing  $\beta$  and  $\gamma$  will broaden the profile, i.e., moving the “valley” further away from the “peak.”

### B. Existence condition and growth rates

The theoretical treatment of the nonlinear Schrödinger equation [Eq. (2)] has been described extensively in the literature. When dispersion and nonlinearity are of the same sign, i.e.,  $\beta\gamma > 0$ , this “self-focusing” (on borrowing a terminology from optics) regime permits modulation instability of the plane-wave train [Eq. (3)] and rogue waves represented by breathers [1,2,5,14,19,20,40]. On the other hand, the “defocusing” regime,  $\beta\gamma < 0$ , will not display these features. Our intention is to elucidate how the boundaries separating these two regimes will be modified if a depth-dependent current is present.

In the parameter regimes with modulation instability, only a finite range of perturbation wave number ( $K$ ) will generate growth for small disturbances:

$$0 < K^2 < 2\gamma S_0/\beta,$$

with the maximum growth rate of  $|\gamma|S_0^2$  occurring at the wave number given by  $K_{\text{critical}} = (\gamma S_0/\beta)^{1/2}$ . For a fixed  $S_0$ , the range of unstable perturbation wave numbers ( $K$ ), or the bandwidth, will depend on the ratio  $(\gamma/\beta)^{1/2}$ . The relationship between the possible occurrence of rogue waves and the growth rates of the perturbations is delicate. The criteria that cause a disturbance from modulation instability to evolve into a rogue wave are complicated, and are only beginning to be appreciated for the nonlinear Schrödinger equation. The modulation instability of the lowest mode on a finite background triggers cascading instabilities and “enslavement” of the higher modes [5]. A “triangular-shaped” spectrum and the formation time of breather modes then follow analytically. Examples of other sophisticated concepts invoked in studying modulation instability include “homoclinic orbits” [41], “super-regular breathers” [42], and patterns of Peregrine breathers [43]. The corresponding pictures for other evolution systems remain challenging issues in research. Two perspectives will be delineated here to enhance the understanding of the intriguing dynamics.

(a) Small disturbances as perturbations on a plane-wave background can amplify only if modulation instability is present for the dynamical system, i.e., for the “focusing regime” of the nonlinear Schrödinger equation in the present case.

(b) However, if this modulation instability is sufficiently strong for a very wide range of wave numbers, perturbations of a large spectrum of length scales may all amplify violently [44]. The magnification of all these background noises and disturbances might mask the actual development of the rogue wave, i.e., create difficulty in identifying the rogue wave in practice.

It will also be instructive to consider how rogue waves can be generated without knowledge of modulation instability. For the Hirota equation, a higher order, “integrable” nonlinear Schrödinger equation with third-order dispersion, localized modes resembling second-order rogue wave solutions can be obtained from numerical marching forward in time with a random or chaotic initial condition [45].

### III. LINEAR SHEAR CURRENT

As a test of the validity of the present algorithm, we apply this formulation to the case of a linear shear current, which has already been studied previously [29,30] using a simplified approach based on the Laplace equation. The linear dispersion relation obtained from Sec. II agrees with the results derived earlier in the literature [29,30]. The numerical results for weak and intermediate strength shear currents are first reported in Secs. III A and III B below. For completeness and future comparison, existing analytical formulations are documented in Sec. III C.

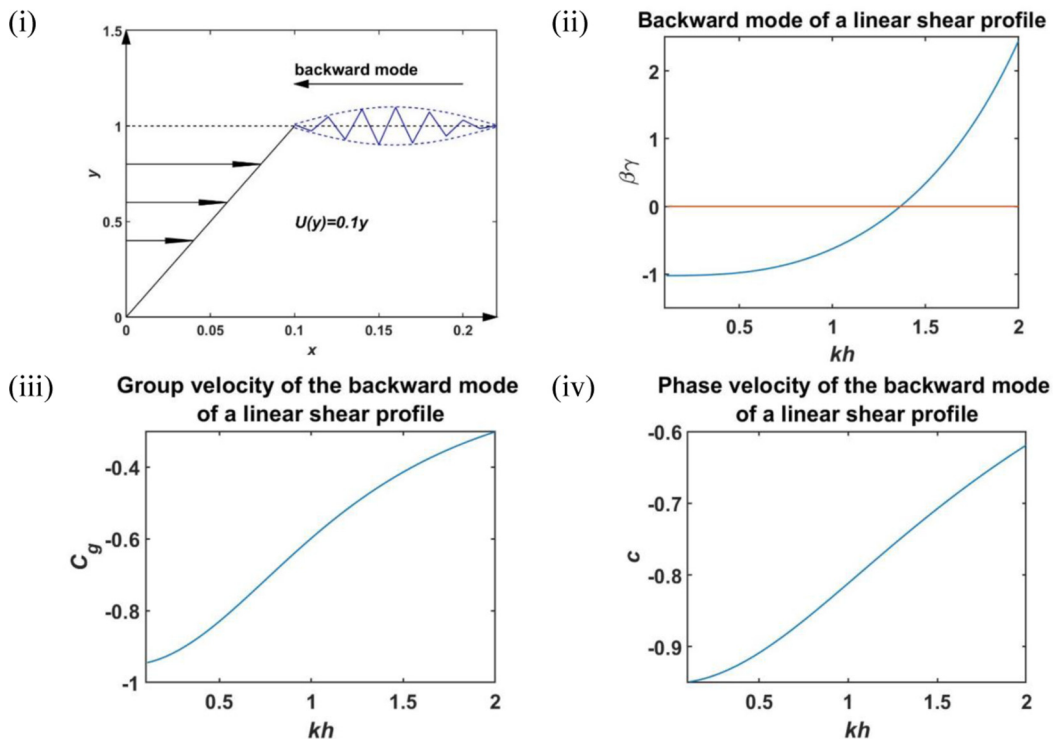


FIG. 2. Relation between the input setting [carrier wave number ( $k$ ), water depth ( $h$ )] and the existence condition of rogue waves ( $\beta\gamma > 0$ ) for the backward mode of a “weak” linear current: (i) the current  $U(y) = 0.1y$ ; (ii) the product  $\beta\gamma$  versus  $kh$ ; (iii) the group velocity ( $c_g$ ) versus  $kh$ ; (iv) the phase speed ( $c$ ) versus  $kh$ . Both  $c$  and  $c_g$  need to be outside the range of the shear velocity ( $[0, 0.1]$  here) to avoid critical level singularities.

In terms of results concerning modulation instability established from previous works [29,30], growth rates should be suppressed for the backward mode (i.e., mode moving against the current). For the forward mode (mode moving with the current), the growth rates increase for small values of  $kh$  and magnitude of shear currents but then subside again if those parameters are large enough. This trend will be illustrated and substantiated here.

In terms of the threshold for the onset of rogue waves, any linear shear will increase the bound of 1.363 numerically. In other words, a deeper fluid is required for these abnormally large waves to occur [29]. We concentrate on the backward mode in this section, as the streamlines may display recirculation regions for this class of modes.

#### A. “Small” linear shear current

For a “small” current  $U(y) = 0.1y$ , the threshold for modulation instability for the backward mode is  $kh = 1.364$  (with a corresponding phase speed  $c = -0.735$ ), very close to the irrotational value of 1.363 (Fig. 2).

For Fig. 2 and all subsequent figures showing the variation of properties with the parameter  $kh$ , we display results starting only at a reasonably small numerical value of, say,  $kh \approx 0.1$  instead of zero. The reason is that, for  $kh$  small, the nonlinear Schrödinger theory breaks down and the dynamics falls into the shallow water regime. The Korteweg–de Vries equation should be used for those small values of  $kh$ .

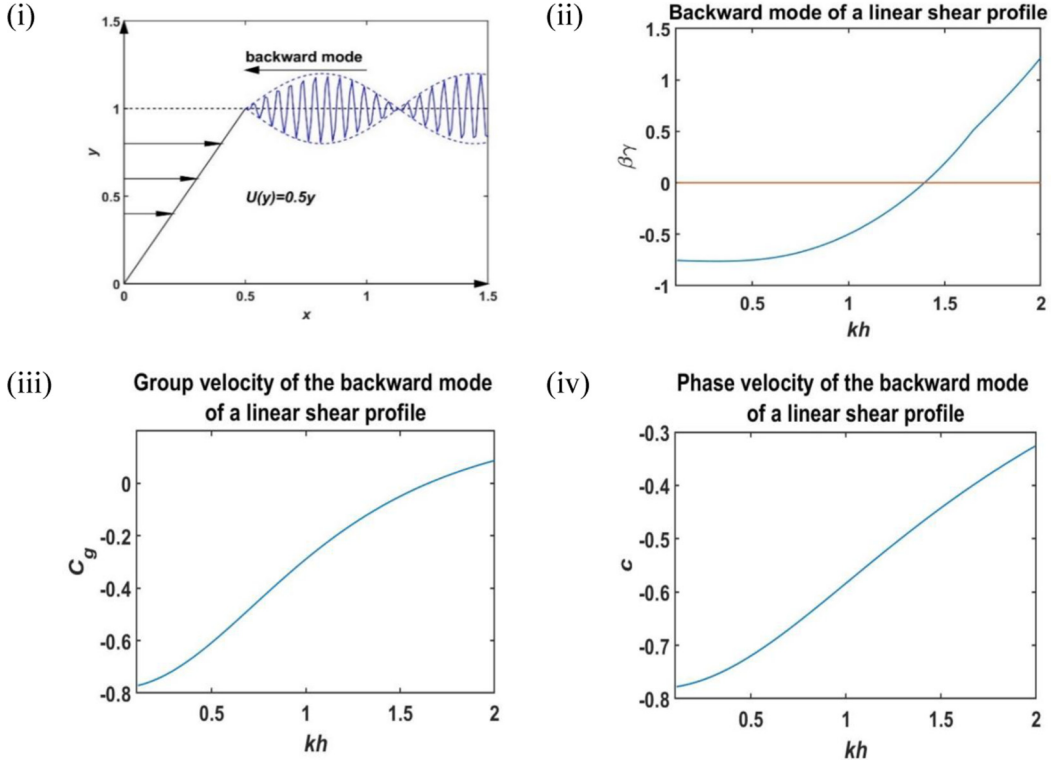


FIG. 3. Relation between the input setting [carrier wave number ( $k$ ), water depth ( $h$ )] and the existence condition of rogue waves ( $\beta\gamma > 0$ ) for the backward mode of an “intermediate” linear current: (i) the current  $U(y) = 0.5y$ ; (ii) the product  $\beta\gamma$  versus  $kh$ ; (iii) the group velocity ( $c_g$ ) versus  $kh$ ; (iv) the phase speed ( $c$ ) versus  $kh$ . Both  $c$  and  $c_g$  need to be outside the range of the shear velocity ( $[0, 0.5]$  here) to avoid critical level singularities.

### B. “Intermediate” linear shear current

When the current is stronger [ $U(y) = 0.5y$ ], modulation instability is further suppressed for the backward mode with rogue wave possible only for  $kh \geq 1.394$  (Fig. 3), in contrast with the irrotational value of 1.363.

If we increase the vorticity further by allowing a still stronger shear current, a phase velocity or group velocity critical level may appear and the analysis becomes much more involved. Even for the present case of  $U(y) = 0.5y$ , a group velocity critical layer will occur at  $kh \approx 1.665$ . In the present context,  $0 \leq U(y) = 0.5y \leq 0.5$ , and hence when the group velocity  $c_g$  goes from a negative value to reach zero, a group velocity critical layer will occur at  $y = 0$  and will continue to arise at other locations as  $c_g$  keeps increasing. Analysis will be more difficult as intermediate terms in the derivation of the nonlinear Schrödinger equation become singular [Eqs. (A11) and (A12) of Appendix B]. We defer these issues to future studies.

For the forward mode of the same shear current, the threshold for modulation instability is now  $kh \geq 1.390$ , which is very close to the threshold of the backward mode.

### C. General formulation for a linear shear current

For the purpose of comparison, analytical formulation for this special case of linear shear obtained earlier in the literature [30] will be tabulated. Our formulation for a general shear profile

produces results consistent with these known equations. The governing equations and coefficients are given by

$$i \frac{\partial B}{\partial \tau} + \alpha \frac{\partial^2 B}{\partial \xi^2} + \delta B^2 B^* = 0,$$

$$\alpha = -\frac{\omega}{k^2} \left\{ \frac{1}{2+X-2\bar{u}} \bar{c}_g^2 + \frac{q[2\sigma^2(1-\bar{u})+X]-2\bar{u}\sigma}{(2+X-2\bar{u})\sigma} \bar{c}_g \right\},$$

$$\delta = -\frac{\omega k^2(1+X-\bar{u})(M+VW)}{8(1-\bar{u})^2(2+X-2\bar{u})\sigma^4} \frac{1}{(1+X-\bar{u})^2},$$

where  $\xi = \varepsilon(x - c_g t)$ ,  $\tau = \varepsilon^2 t$ ,  $B = A(1 + X - \bar{u})$  ( $A$  = wave amplitude),  $\bar{c}_g = c_g k / \omega$ ,

$$X = \sigma \bar{\Omega}, \quad \bar{\Omega} = \frac{\Omega}{\omega}, \quad \sigma = \tanh q, \quad q = kh, \quad \bar{u} = \frac{U_0}{c}, \quad c = \frac{\omega}{k}.$$

$M$  can be written as a lengthy expression in Appendix A, while  $V$  and  $W$  are given by

$$V = \{[1 + \bar{u}(\bar{u} - 2 - 2X \cosh^2 q)] \cosh^{-2} q + X(X + 2)\} (\bar{c}_g + \bar{\Omega} q)$$

$$+ (1 + X - \bar{u})(2 + X - 2\bar{u})(1 - \bar{u}), \quad W = \frac{W_1}{W_2},$$

$$W_1 = 2(1 - \bar{u})\sigma^2 [(1 - \bar{u})(\bar{c}_g - \bar{u}) + (1 + X - \bar{u})(2 + X - 2\bar{u})(1 - \bar{u}) \cosh^2 q],$$

$$W_2 = \left[ (\bar{c}_g - \bar{u})(\bar{c}_g + \bar{\Omega} q) - (1 + X - \bar{u})(1 - \bar{u}) \frac{q}{\sigma} \right] \cosh^2 q.$$

The velocity profile is  $U_0 + \Omega(y - h)$  for a fluid located between  $y = 0$  and  $y = h$ . In the rest of this paper, we have set  $h = 1$ , and adjusted  $U_0$  and  $\Omega$  to attain a profile of  $U(y) = by$ ,  $b$  = a real parameter.

#### IV. SHEAR CURRENTS WITH NONZERO VORTICITY GRADIENT

##### A. Shear profile concave to the right, forward mode

When the current profile is concave to the right (abbreviated below as a “*concave current*”) with  $U(y) = 0.5y^2$  being chosen as an illustrative example, the condition for modulation instability for the forward mode is  $kh \geq 1.269$ , by performing the sequence of calculations outlined in Appendix B. This is lower than the threshold for the irrotational case of  $kh \geq 1.363$  by roughly 7% for the present case of a Froude number of 0.5 (measured by the surface velocity divided by the square root of the product of gravity and water depth) (Fig. 4). In other words, a concave profile enlarges the regime of occurrence of rogue waves by allowing a smaller water depth requirement compared with the irrotational case. As the background shear velocity is in the range of (0,0.5), there is no critical layer for these parameters.

##### B. Shear profile concave to the right, backward mode

For the backward mode of the same concave current  $U(y) = 0.5y^2$ , the existence condition for rogue waves or modulation instability is  $kh \geq 1.518$  (Fig. 5). The overall trends for a concave current and a linear current are thus different, as rogue waves can occur for a smaller depth for the forward mode ( $kh$  threshold smaller), but the opposite is true for the backward mode ( $kh$  threshold bigger). Moreover, this “stabilizing” effect of a concave current is much stronger than a linear shear current (1.518 versus 1.394 with 1.363 as the irrotational flow benchmark value, i.e., 11.37% versus 2.27%), for the present case of the Froude number being 0.5 (i.e., maximum current velocity of 0.5 at the free surface). A group velocity critical layer appears at  $kh = 1.845$ .

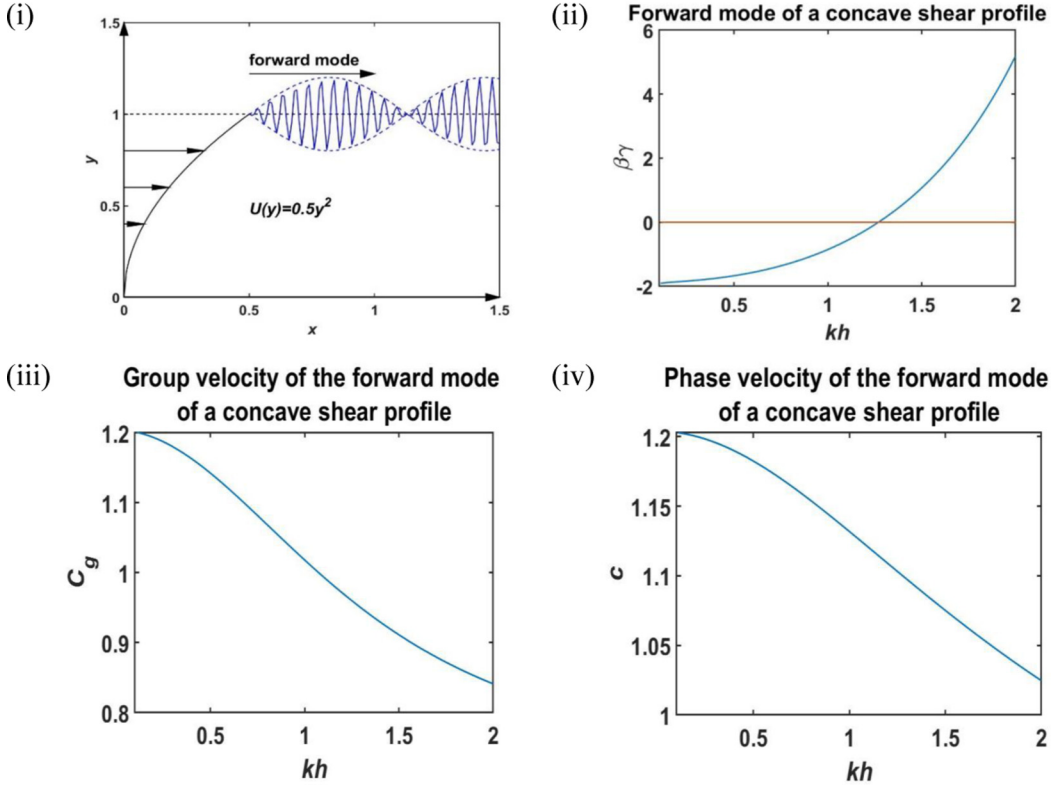


FIG. 4. The dynamics of modulation instability for a *forward* mode of a *concave* shear current: (i) the background velocity profile; (ii) product of the dispersive ( $\beta$ ) and nonlinear ( $\gamma$ ) coefficients, positive for rogue wave occurrence; (iii) variation of the group velocity ( $c_g$ ) with  $kh$ ; (iv) variation of the phase velocity ( $c$ ) with  $kh$ . Both  $c$  and  $c_g$  need to be outside the range of the shear velocity ( $[0,0.5]$  here) to avoid critical level singularities.

### C. Shear profile convex to the right, forward mode

When the current profile is convex to the right (abbreviated below as a “*convex current*”), a different picture emerges. For comparison we again choose a current profile with maximum velocity of 0.5 at the free surface, with  $U(y) = y - 0.5y^2$  being a typical example. The same sequence of calculations described in Appendix B can be repeated. For the forward mode, the threshold for modulation instability is now  $kh \geq 1.507$ , i.e., a deeper fluid is required for rogue waves to occur in the forward mode with the presence of a convex current (Fig. 6).

### D. Shear profile convex to the right, backward mode

For the same convex current as given in Sec. IV C above, the backward mode now yields a lower threshold (smaller fluid depth) for modulation instability to occur, namely,  $kh \geq 1.323$  (Fig. 7).

However, in the present case, a group velocity critical layer will occur soon after the threshold of modulation instability, namely, at  $kh \approx 1.465$ .

## V. GROWTH RATE ANALYSIS

The presence of modulation instability is necessary for the evolution of a breather-type solution, which is our definition of a rogue wave within the nonlinear Schrödinger-type model. Rogue waves

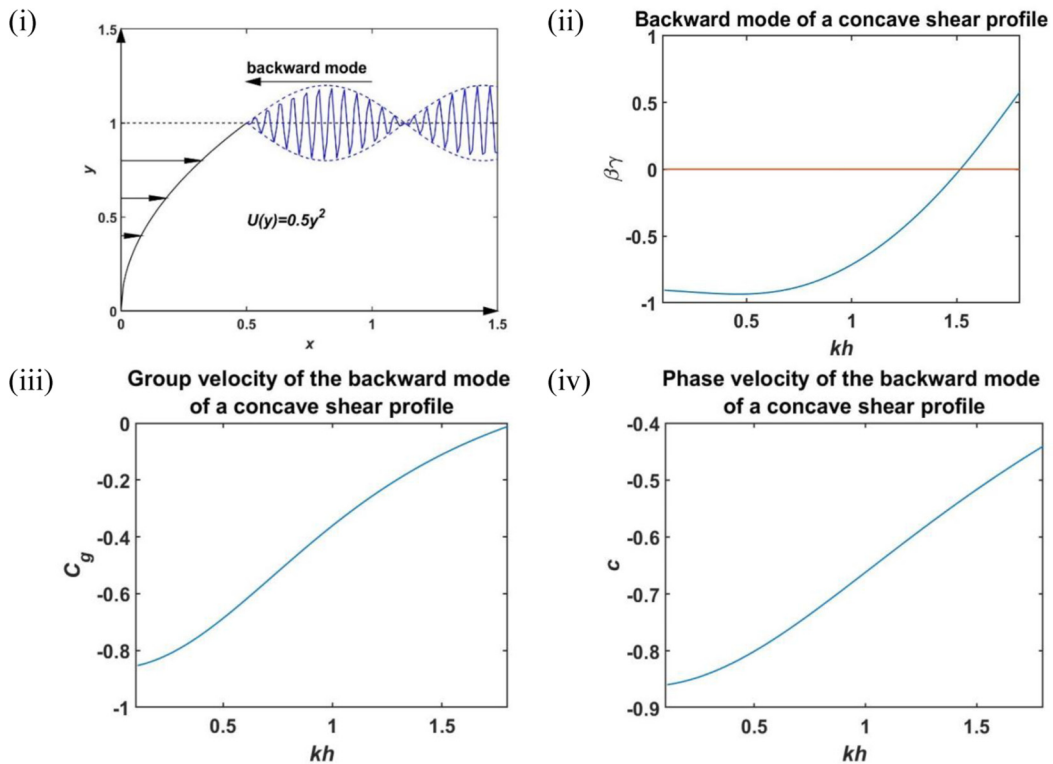


FIG. 5. The dynamics of modulation instability for a *backward* mode of a *concave* shear current: (i) the background velocity profile; (ii) product of the dispersive ( $\beta$ ) and nonlinear ( $\gamma$ ) coefficients, positive for rogue wave occurrence; (iii) variation of the group velocity ( $c_g$ ) with  $kh$ ; (iv) variation of the phase velocity ( $c$ ) with  $kh$ . Both  $c$  and  $c_g$  need to be outside the range of the shear velocity ( $[0, 0.5]$  here) to avoid critical level singularities.

can only be possible for the nonlinear Schrödinger equation [Eq. (2)] if the condition  $\beta\gamma \geq 0$  holds. However, for a fixed plane-wave amplitude  $S_0$ , the growth rates of perturbations will only depend on the absolute value of  $\gamma$ . Furthermore, the range of unstable perturbation wave numbers ( $K$ ), or the bandwidth, will depend on the ratio  $(\gamma/\beta)^{1/2}$ .

Physically, modulation instabilities of sufficiently strong magnitude for a wide spectrum of wavelengths might mask the growth and decay cycle of the rogue wave, as background noise of various wavelengths, not just the long ones, might grow too (see discussion in Sec. II). Here we illustrate this scenario through studying families of shear flows by varying the current parameters. The growth rate parameter  $\gamma$  is computed and thus correlation with the likelihood of observing rogue waves is made. For normalization purposes, it will be appropriate to compare the resulting growth rates with a reference benchmark. For this purpose, the growth rate in the absence of shear flow, or the growth rate for irrotational flows,  $\gamma_{\text{no shear}}$ , will be chosen. All growth rate data ( $\gamma$ ) presented below will be compared with this reference mark.

### A. Linear shear current

We consider a family of linear currents  $U(y) = by$  with real parameter  $b$ . The maximum growth rate as measured by the parameter  $|\gamma|S_0^2$  as a function of  $b$  for typical values of  $S_0 (=1)$  and  $kh (=1.5)$  is shown in Fig. 8. Negative values of  $b$  (linear current going to the left) effectively represent the case of backward modes. The trend is consistent with results found earlier in the

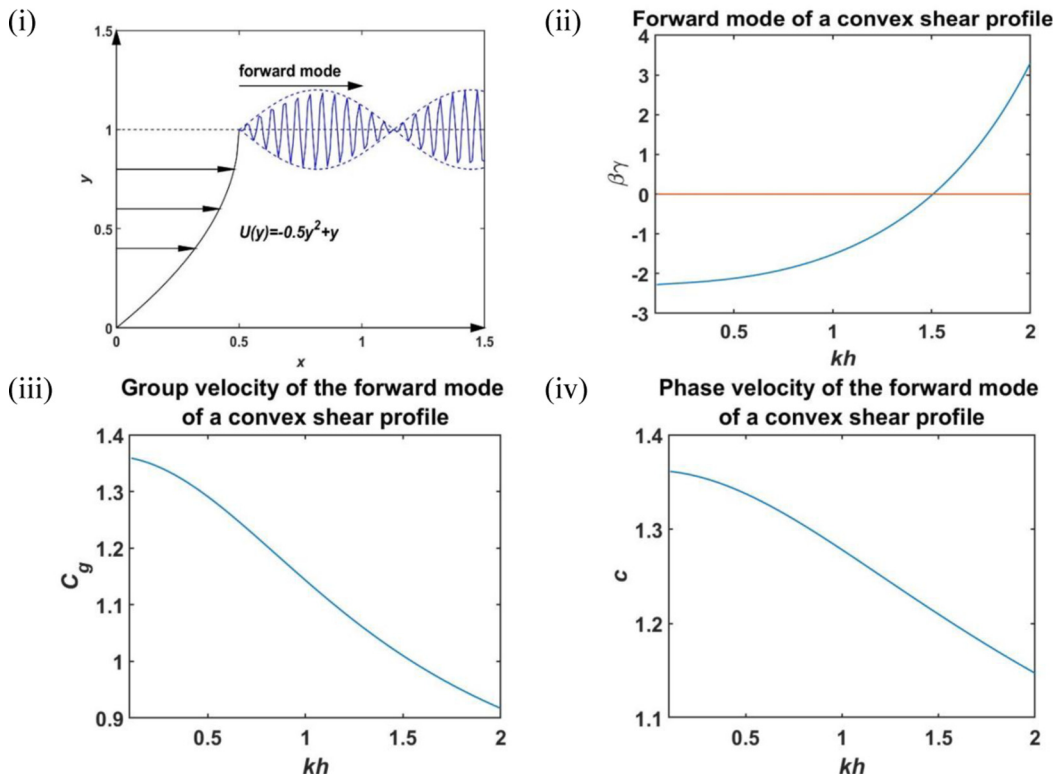


FIG. 6. The dynamics of modulation instability for a *forward* mode of a *convex* shear current: (i) the background velocity profile; (ii) product of the dispersive ( $\beta$ ) and nonlinear ( $\gamma$ ) coefficients, positive for rogue wave occurrence; (iii) variation of the group velocity ( $c_g$ ) with  $kh$ ; (iv) variation of the phase velocity ( $c$ ) with  $kh$ . Both  $c$  and  $c_g$  need to be outside the range of the shear velocity ( $[0,0.5]$  here) to avoid critical level singularities.

literature, namely, growth rates (i) decrease for the backward mode and (ii) increase first but then subside for the forward mode, as the shear strength is varied.

### B. Concave shear profiles

As a typical example for concave profiles, we choose  $U(y) = by^2$ . We compute the growth rates of perturbations for various concave shear profiles by varying the real parameter  $b$  with a fixed value of  $kh = 1.5$ . We again normalize the growth rates using the value with no shear (i.e.,  $b = 0$ , or value for irrotational flow) as a benchmark. Generally the growth rates get bigger as we increase the values of  $b$  from zero. Beyond a value of  $b \approx 1.4$ , this growth rate subsides (Fig. 9). If we compare these results with those of a linear shear with the same velocities at the two boundaries ( $0, b$  at  $y = 0, 1$ , respectively), the growth rates of perturbations for the concave currents are significantly larger.

### C. Convex shear profiles

For standardization purposes, we select  $U(y) = b(-0.5y^2 + y)$  with varying  $b$  but a fixed  $kh = 1.5$  as the test case for convex profiles. The maximum growth rate as a function of  $b$  is then illustrated in Fig. 10, with a growth rate smaller than that of a linear shear, in line with the results of Sec. IV.

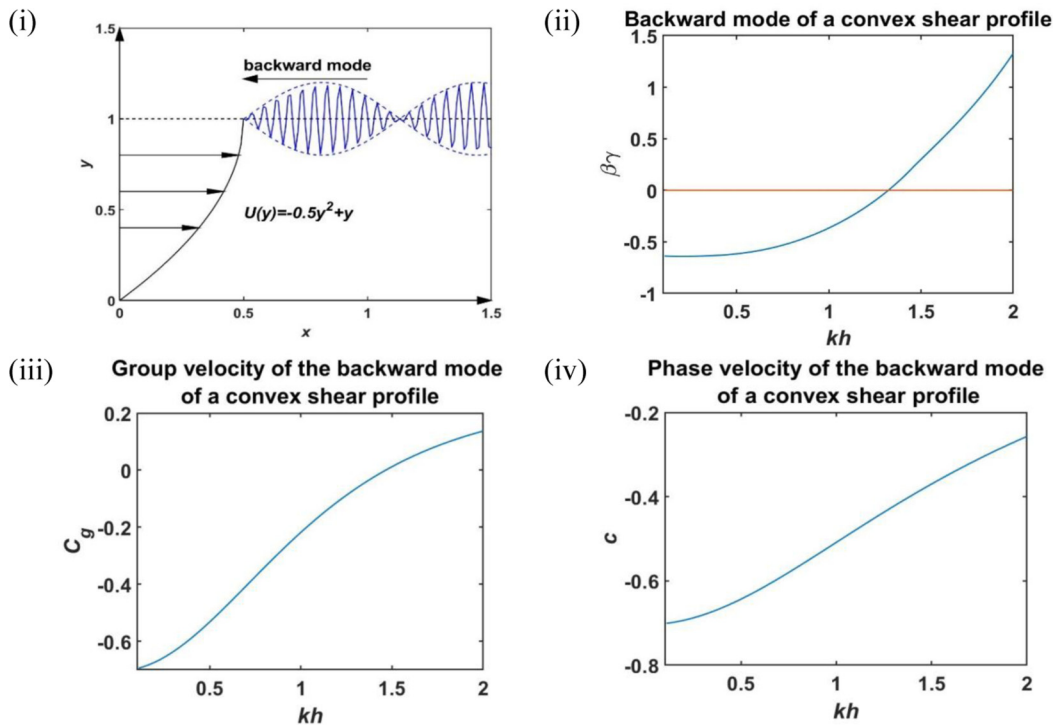


FIG. 7. The dynamics of modulation instability for a *backward* mode of a *convex* shear current: (i) the background velocity profile; (ii) product of the dispersive ( $\beta$ ) and nonlinear ( $\gamma$ ) coefficients, positive for rogue wave occurrence; (iii) variation of the group velocity ( $c_g$ ) with  $kh$ ; (iv) variation of the phase velocity ( $c$ ) with  $kh$ . Both  $c$  and  $c_g$  must be outside the range of the shear velocity to avoid critical level singularities.

## VI. PRELIMINARY STUDIES ON STREAMLINE PATTERNS ASSOCIATED WITH ROGUE WAVES

Conventional understanding of particle motions for small amplitude waves is that the path is elliptic (circular) for a fluid of finite (infinite) depth [46]. At second order in wave amplitude, a nonzero mean transport, the “Stokes drift,” exists due to wave self-interaction. However, recent studies show that the situation might be more intriguing than this simple picture. Moreover, the locations of maximum local pressure need not be confined to those places at the seabed beneath the wave crest, i.e., the scenario of “pressure anomaly” may occur [27,46,47]. Naturally, if we incorporate a linear shear current, the analysis will be even more involved [46–48]. Most investigations on the streamline patterns in the literature focus on traveling or periodic waves for free surface flows with or without shear currents. In particular, in a frame of reference traveling with a solitary wave, the backward mode for a linear current profile can exhibit recirculation regions [31]. The corresponding results for transient modes like rogue waves apparently have not yet been given. The goal here is to conduct a preliminary examination on this issue.

We shall plot the streamline patterns by employing a stream function  $\Psi$  defined in the usual way, namely,  $\Psi_y = u$ ,  $\Psi_x = -v$ . The curves termed as “streamlines” in this context must have orientation of the tangent being aligned with the direction of the velocity field. We calculate the perturbation series to leading order and this streamline pattern is illustrated for the total stream function (shear flow and the wave field) (Fig. 11). For large values of time (say  $t = \pm 10\,000$ ), the fluid exhibits approximately a sinusoidal flow field being advected by a parallel shear flow. At finite values of

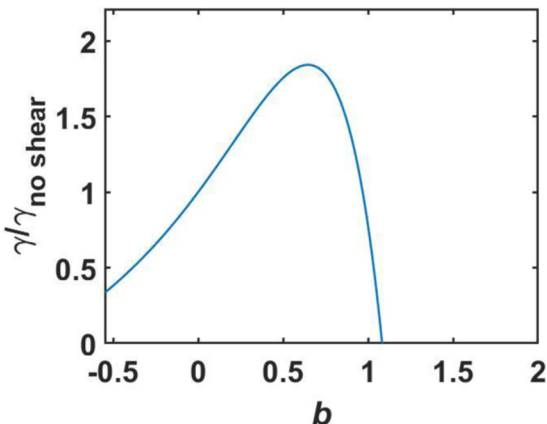


FIG. 8. The variation of the maximum growth rate with changing strength of a linear current  $U(y) = by$  for  $kh = 1.5$ . This growth rate ( $\gamma$ ) is normalized by the corresponding growth rate in the absence of shear ( $\gamma_{\text{no shear}}$ ).

time, the rogue wave displays an abrupt growth and decay phase, the benchmark of this type of motion.

## VII. DISCUSSION AND CONCLUSIONS

The analysis of free surface flows with arbitrary depth-dependent shear profile is considerably more complicated than that of the linear shear case, both theoretically and computationally. To leading order the evolution of a narrow-band wave packet is governed by the nonlinear Schrödinger equation, with dispersion and cubic nonlinearity being of the same sign as necessary for the onset of modulation instability and as an existence criterion for rogue waves. The present studies show that these criteria depend critically on the precise shape of the shear profile, with perhaps significant implications in terms of issues in practical applications like marine operations and wave generation by wind. More precisely, these results can be elucidated through these perspectives:

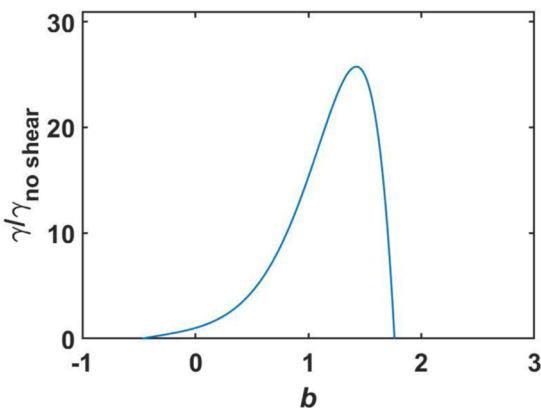


FIG. 9. The variation of the maximum growth rate with changing strength of concave currents  $U(y) = by^2$  for varying  $b$  and  $kh = 1.5$ . This growth rate ( $\gamma$ ) is normalized by the corresponding growth rate in the absence of shear ( $\gamma_{\text{no shear}}$ ).

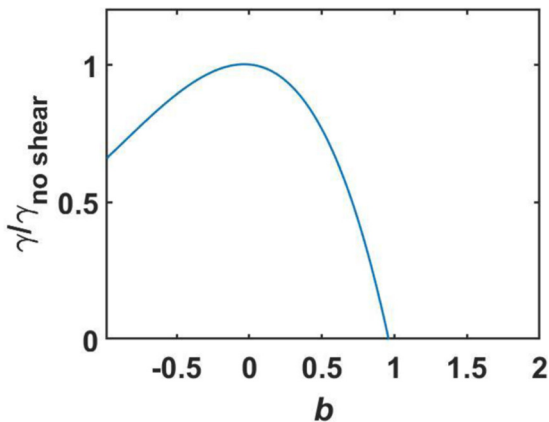


FIG. 10. The variation of the maximum growth rate with changing strength of convex currents  $U(y) = b(y - 0.5y^2)$  for varying  $b$  and  $kh = 1.5$ . This growth rate ( $\gamma$ ) is normalized by the corresponding growth rate in the absence of shear ( $\gamma_{\text{no shear}}$ ).

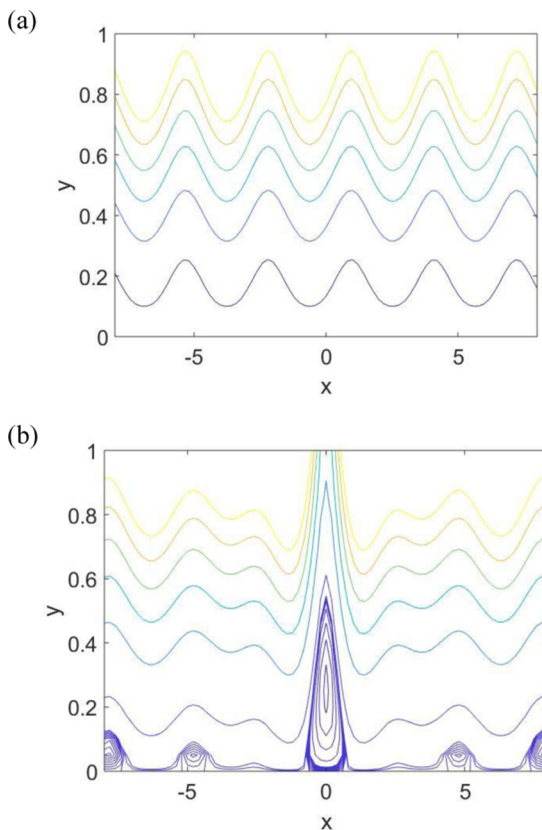


FIG. 11. Streamline patterns for a rogue wave for a backward mode in a linear shear flow  $U(y) = 0.4y$  (mode going against the current). (a) Time  $t = \pm 10000$ , (b)  $t = 0$ , with input parameters  $S_0 = 1$ ,  $\varepsilon = 0.03$ ,  $k = 2$ ,  $h = 1$ ,  $c = -0.397$ ,  $c_g = -0.0104$ ,  $\beta = 0.0948$ ,  $\gamma = 19.067$ .

(1) For the irrotational case, an occurrence of rogue waves requires a deep fluid with the threshold being  $kh \approx 1.363$ . With a linear shear current, the numerical bound of 1.363 is increased for both the forward and backward modes, i.e., a greater fluid depth is necessary. However, the growth rates behave in a different manner.

(2) For profiles with nonzero vorticity gradient, modulation instability will require a smaller (larger) fluid depth for the forward (backward) mode, respectively, in the presence of a concave current. The opposite is true for a convex current.

(3) The growth rates of modulation instability for concave currents are much bigger than those of linear and convex currents.

(4) Previous studies of streamline patterns in the literature mostly focus on the steady cases of solitary or periodic waves. We have extended these considerations to rogue waves in a preliminary study. Not surprisingly, the streamlines exhibit a large transient sequence of motions at a finite time but eventually decay back to a tranquil background.

We anticipate exciting paths in future research efforts with these possible directions:

(1) For analytical simplicity, only quadratic polynomials have been employed as representative examples of convex and concave currents. Other velocity profiles should be tested.

(2) A more penetrating study on stagnation points and recirculation regions should be conducted [31,47,48].

(3) The issue of pressure anomaly should be addressed. The possible existence of local maximum or minimum of pressure in the interior of a fluid should be investigated [27,47].

(4) The presence of critical level will affect the dynamics, but the details are largely unexplored [49].

(5) Extensions to other flow settings, e.g., dynamics of stratified fluids, will definitely be valuable [50].

#### ACKNOWLEDGMENTS

Partial financial support has been provided by the Research Grants Council General Research Fund Contracts No. HKU17200815 and No. HKU17200718 (Q.P. and K.W.C.), as well as the Leverhulme Fellowship EM-2015-37 (RHJG).

#### APPENDIX A

The parameter  $M$  in Sec. III C is given by the lengthy expression

$$\begin{aligned}
 M = & (\cosh 4q + 8 - 2\sigma^2)\cosh^{-4}q - (5\cosh^{-2}q - 26)X^3 + 3(5\cosh^{-4}q - 4\cosh^{-2}q + 8)X \\
 & - (2\cosh^{-2}q - 9)X^4 + (4\cosh^{-4}q - 5\cosh^{-2}q + 34)X^2 + X^5 \\
 & + \bar{u}[-5(2\cosh^{-4}q + 7\cosh^{-2}q - 8)\cosh^{-2}q - 40 - 12X(5\cosh^{-4}q - 4\cosh^{-2}q + 8) \\
 & - 3X^2(4\cosh^{-4}q - 5\cosh^{-2}q + 34) + 2X^3(5\cosh^{-2}q - 26) + X^4(2\cosh^{-2}q - 9)] \\
 & + \bar{u}^2[10(2\cosh^{-4}q + 7\cosh^{-2}q - 8)\cosh^{-2}q + 80 + 18X(5\cosh^{-4}q - 4\cosh^{-2}q + 8) \\
 & + 3X^2(4\cosh^{-4}q - 5\cosh^{-2}q + 34) + X^3(-5\cosh^{-2}q + 26)] \\
 & + \bar{u}^3[-10(2\cosh^{-4}q + 7\cosh^{-2}q - 8)\cosh^{-2}q - 80 - 12X(5\cosh^{-4}q - 4\cosh^{-2}q + 8) \\
 & - X^2(4\cosh^{-4}q - 5\cosh^{-2}q + 34)] + \bar{u}^4[5(2\cosh^{-4}q + 7\cosh^{-2}q - 8)\cosh^{-2}q \\
 & + 40 + 3X(5\cosh^{-4}q - 4\cosh^{-2}q + 80)] - \bar{u}^5(\cosh 4q + 8 - 2\sigma^2)\cosh^{-4}q.
 \end{aligned}$$

#### APPENDIX B

With gravity and density being normalized to unity, the governing equations are based on the usual principle of mass and momentum conservation:

$$u_x + v_y = 0, \quad u_t + uu_x + vv_y = -p_x, \quad v_t + uv_x + vv_y = -p_y - 1. \quad (\text{B1})$$

The boundary conditions are no flow through the rigid bottom at  $y = 0$ , kinematic condition at the free surface at  $y = 1 + \eta$ , and constant pressure at the free surface. The velocity components  $u$ ,  $v$ ,

the free surface elevation  $\eta$ , and the pressure  $p$  are expanded as (c.c. = complex conjugate)

$$\begin{aligned} u &= U(y) + \varepsilon(u_1 e^{i\theta} + \text{c.c.}) + \varepsilon^2(u_0 + u_2 e^{2i\theta} + \text{c.c.}) + \cdots, \\ v &= \varepsilon(v_1 e^{i\theta} + \text{c.c.}) + \varepsilon^2(v_2 e^{2i\theta} + \text{c.c.}) + \varepsilon^3(v_0 + v_3 e^{3i\theta} + \text{c.c.}) + \cdots, \\ p &= 1 - y + \varepsilon(p_1 e^{i\theta} + \text{c.c.}) + \varepsilon^2(p_0 + p_2 e^{2i\theta} + \text{c.c.}) + \cdots, \\ \eta &= \varepsilon(\eta_1 e^{i\theta} + \text{c.c.}) + \varepsilon^2(\eta_0 + \eta_2 e^{2i\theta} + \text{c.c.}) + \cdots, \end{aligned} \quad (\text{B2})$$

where  $\theta = k(x - ct)$  represents the fast oscillations and the small parameter  $\varepsilon$  measures the amplitude. The slow variables  $X$  and  $T$  are defined by the relation  $(X, T) = \varepsilon(x, t)$ .

Terms with appropriate powers of  $\varepsilon$  are collected in straightforward but lengthy calculations. For compact notations, we further introduce coordinates through  $X - c_g T$  by  $\xi$  and  $\varepsilon T$  by  $\tau$ , where  $c_g$  is the group velocity. Physically we are now in a frame moving with the group velocity. The appropriate expansion is then given by

$$v_1 = ikS\phi_{01}(y) + \varepsilon \frac{\partial S}{\partial \xi} \phi_{11}(y) + \frac{\varepsilon^2}{ik} \frac{\partial^2 S}{\partial \xi^2} \phi_{21}(y) + ik\varepsilon^2 [S^2 S^* \phi_{41}(y) + L_1 S \phi_{51}(y) + L_1 S \phi_{61}(y)]$$

and

$$\begin{aligned} v_2 &= ikS^2 \phi_2(y), \quad v_0 = \frac{\partial(SS^*)}{\partial \xi} v_{00}(y) + \frac{\partial L_1}{\partial \xi} v_{20}(y), \\ u_0 &= SS^* U_{00}(y) + L_1 U_{10}(y) + L_1 U_{20}(y), \end{aligned} \quad (\text{B3})$$

where  $S, L_1$  are all functions of  $\xi$  and  $\tau$ . These functions are related by the equations

$$\frac{\partial S}{\partial \tau} = i \left[ \beta_1 \frac{\partial^2 S}{\partial \xi^2} + \gamma_0 S^2 S^* + (\gamma_1 + \gamma_2) L_1 S \right], \quad \alpha \frac{\partial^2 L_1}{\partial \xi^2} = \delta_1 \frac{\partial^2(SS^*)}{\partial \xi^2}. \quad (\text{B4})$$

The nonlinear Schrödinger equation could thus be obtained as

$$i \frac{\partial S}{\partial \tau} + \beta \frac{\partial^2 S}{\partial \xi^2} + \gamma S^2 S^* = 0, \quad (\text{B5})$$

where  $\beta = \beta_1$ ,  $\gamma = \gamma_0 + (\gamma_1 + \gamma_2) \frac{\delta_1}{\alpha}$ .

These coefficients are determined by solving a sequence of boundary value problems starting with the vertical structure of the linear eigenfunction being governed by the Rayleigh equation

$$\frac{d^2 \phi_{01}}{dy^2} - \left( k^2 + \frac{U''}{U_c} \right) \phi_{01} = 0, \quad (\text{B6a})$$

subject to the boundary conditions

$$\phi_{01} = 0, \quad y = 0, \quad (\text{B6b})$$

$$\frac{d\phi_{01}}{dy} - \left( \frac{U'}{U_c} + \frac{1}{U_c^2} \right) \phi_{01} = 0, \quad y = 1, \quad (\text{B6c})$$

with Eq. (B6c) being obtained by combining the kinematic and dynamic boundary conditions. Calculations at the next order proceed in a similar manner:

$$\frac{d^2 \phi_{11}}{dy^2} - \left( k^2 + \frac{U''}{U_c} \right) \phi_{11} = \left( 2k^2 - (c - c_g) \frac{U''}{U_c^2} \right) \phi_{01}, \quad (\text{B7a})$$

$$\phi_{11} = 0, \quad y = 0, \quad (\text{B7b})$$

$$\frac{d\phi_{11}}{dy} - \left( \frac{U'}{U_c} + \frac{1}{U_c^2} \right) \phi_{11} = (c_g - c) b_1 \phi_{01}, \quad y = 1, \quad (\text{B7c})$$

where  $c_g$  is group velocity given by

$$c_g = c - \frac{2k^2}{D} \int_0^1 \phi_{01}^2 dy \quad (\text{B7d})$$

with

$$D = \int_0^1 \frac{U''}{U_c^2} \phi_{01}^2 dy - b_1 \phi_{01}^2(1). \quad (\text{B7e})$$

The second-order dispersion coefficient is then obtained at the next order as

$$\beta_1 = \frac{1}{kD} \left[ \begin{aligned} &(c - c_g) \{ [b_1 + b_2(c - c_g)] \phi_{01}^2(1) - b_1 \phi_{11}(1) \phi_{01}(1) \} \\ &- \int_0^1 \left\{ k^2 + \frac{(c - c_g) U''}{U_c^2} \left( 1 + \frac{(c - c_g)}{U_c} \right) \right\} \phi_{01}^2 dy \\ &- \int_0^1 \left( 2k^2 - \frac{(c - c_g) U''}{U_c^2} \right) \phi_{01} \phi_{11} dy \end{aligned} \right]. \quad (\text{B8})$$

The computations of the nonlinear terms start with the second harmonic through the system:

$$\frac{d^2 \phi_2}{dy^2} - \left( 4k^2 + \frac{U''}{U_c} \right) \phi_2 = -\frac{1}{U_c} \left( \frac{U''}{U_c} \right)' \phi_{01}^2, \quad (\text{B9a})$$

with boundary conditions

$$\phi_2 = 0, \quad y = 0, \quad (\text{B9b})$$

$$\frac{d\phi_2}{dy} - \left( \frac{U'}{U_c} + \frac{1}{U_c^2} \right) \phi_2 = -b_5 \phi_{01}^2, \quad y = 1. \quad (\text{B9c})$$

The mean flow distribution is found from similar calculations:

$$\left( \frac{\partial}{\partial \tau} + U \frac{\partial}{\partial \xi} \right) \frac{\partial v_0}{\partial y} - U' \frac{\partial v_0}{\partial \xi} - \frac{\partial^2 \eta_0}{\partial \xi^2} + f_1(y) \frac{\partial^2}{\partial \xi^2} (SS^*) = 0, \quad (\text{B10a})$$

where the functions  $f_1(y)$  and  $f_2(y)$  are determined by the expressions

$$f_1(y) = \left( k^2 + U_g \frac{U''}{U_c^2} \right) \phi_{01}^2 - \left( \frac{d\phi_{01}}{dy} \right)^2, \quad (\text{B10b})$$

$$f_2(y) = k^2 \phi_{01}^2 - \left( \frac{d\phi_{01}}{dy} - \frac{U'}{U_c} \phi_{01} \right)^2. \quad (\text{B10c})$$

The auxiliary coefficients are represented as

$$v_{00} = -U_g \int_0^y \frac{f_1}{U_g^2} dy, \quad v_{20} = U_g \int_0^y \frac{dy}{U_g^2}, \quad v_{30} = -U_g \int_0^y \frac{f_2}{U_g^2} dy, \quad (\text{B11})$$

with  $U_g = U(y) - c_g$ . The corresponding mean flow components are given by

$$U_{00} = \frac{1}{U_g} (f_1 - U' v_{00}), \quad U_{10} = -\frac{1}{U_g}, \quad U_{20} = -\frac{U' v_{20}}{U_g}, \quad U_{30} = -\frac{U' v_{30}}{U_g}. \quad (\text{B12})$$

Substituting these expressions into the mean flow boundary conditions finally leads to expressions for  $\alpha$ ,  $\delta_1$ , and  $\delta_2$ :

$$\begin{aligned} \alpha &= 1 - \left( \int_0^1 \frac{dy}{U_g^2} \right)^{-1}, \quad \delta_1 = \left( \int_0^1 \frac{dy}{U_g^2} \right)^{-1} \left( \int_0^1 \frac{f_1}{U_g^2} dy - \frac{b_1 \phi_{01}^2(1)}{U_g(1)} \right), \\ \delta_2 &= \left( \int_0^1 \frac{dy}{U_g^2} \right)^{-1} \left( \int_0^1 \frac{f_2}{U_g^2} dy \right). \end{aligned} \quad (\text{B13})$$

The constants  $\gamma_j$  are found by solvability requirements for the nonlinear corrections through the classical Fredholm alternative theorem:

$$\begin{aligned}\gamma_0 &= \frac{k}{D} \left[ \int_0^1 \left( \frac{U_{00}''}{U_c} - \frac{U''}{U_c^2} U_{00} \right) \phi_{01}^2 dy - \frac{1}{2} \int_0^1 \frac{1}{U_c} \left( \frac{U''}{U_c} \right)' \phi_2 \phi_{01}^2 dy \right. \\ &\quad \left. - \int_0^1 \frac{1}{U_c^2} \left( \frac{U''}{U_c} \right)' \phi_{01}^2 (\phi_{01}^2)' dy - \frac{1}{2} \int_0^1 \frac{1}{U_c} \left\{ \frac{1}{U_c} \left( \frac{U''}{U_c} \right) \right\}' \phi_{01}^4 dy \right. \\ &\quad \left. - \left[ (b_3 U_{00}' - b_1 U_{00}) \phi_{01}^2 - \frac{b_5}{2} \phi_2 \phi_{01}^2 + \frac{b_6}{2} \phi_{01}^4 \right]_{y=1} \right], \\ \gamma_1 &= \frac{k}{D} \left[ \int_0^1 \left( \frac{U_{10}''}{U_c} - \frac{U''}{U_c^2} U_{10} \right) \phi_{01}^2 dy - \left[ (b_3 U_{10}' - b_1 U_{10} - b_4) \phi_{01}^2 \right]_{y=1} \right], \\ \gamma_2 &= \frac{k}{D} \left[ \int_0^1 \left( \frac{U_{20}''}{U_c} - \frac{U''}{U_c^2} U_{20} \right) \phi_{01}^2 dy - \left[ (b_3 U_{20}' - b_1 U_{20}) \phi_{01}^2 \right]_{y=1} \right].\end{aligned}\tag{B14}$$

Here the compact notations for the auxiliary coefficients are

$$\begin{aligned}U_c &= U(y) - c, \quad b_1 = \left[ \frac{U'}{U_c^2} + \frac{2}{U_c^3} \right]_{y=1}, \quad b_2 = \left[ \frac{U'}{U_c^3} + \frac{3}{U_c^4} \right]_{y=1}, \\ b_3 &= \left[ \frac{1}{U_c} \right]_{y=1}, \quad b_4 = \left[ k^2 - \frac{1}{U_c^4} \right]_{y=1}, \\ b_5 &= \left[ \frac{3k^2}{U_c} + \frac{U''}{U_c^2} - \frac{(U')^2}{U_c^3} - \frac{3U'}{U_c^4} - \frac{3}{U_c^5} \right]_{y=1}, \\ b_6 &= \left[ -\frac{2k^2 U'}{U_c^3} - \frac{U'''}{U_c^3} + \frac{(U')^3}{U_c^5} + \frac{5(U')^2}{U_c^6} + \frac{10U'}{U_c^7} + \frac{8}{U_c^8} \right]_{y=1}.\end{aligned}\tag{B15}$$

- 
- [1] A. D. D. Craik, *Wave Interactions and Fluid Flows* (Cambridge University Press, Cambridge, 1985).  
 [2] C. C. Mei, *The Applied Dynamics of Ocean Surface Waves* (World Scientific, Singapore, 1989).  
 [3] J. M. Dudley, F. Dias, M. Erkintalo, and G. Genty, Instabilities, breathers and rogue waves in optics, *Nat. Photonics* **8**, 755 (2014).  
 [4] F. Fedele, On certain properties of the compact Zakharov equation, *J. Fluid Mech.* **748**, 692 (2014).  
 [5] S. A. Chin, O. A. Ashour, and M. R. Belic, Anatomy of the Akhmediev breather: Cascading instability, first formation time, and Fermi-Pasta-Ulam recurrence, *Phys. Rev. E* **92**, 063202 (2015).  
 [6] J. Thomas and R. Yamada, An amplitude equation for surface gravity wave-topography interactions, *Phys. Rev. Fluids* **3**, 124802 (2018).  
 [7] K. B. Dysthe, Note on a modification to the non-linear Schrödinger equation for application to deep-water waves, *Proc. R. Soc. A* **369**, 105 (1979).  
 [8] O. Gramstad and K. Trulsen, Fourth-order coupled nonlinear Schrödinger equations for gravity waves on deep water, *Phys. Fluids* **23**, 062102 (2011).  
 [9] A. Armaroli, D. Eeltink, M. Brunetti, and J. Kasparian, Nonlinear stage of Benjamin-Feir instability in forced/damped deep-water waves, *Phys. Fluids* **30**, 017102 (2018).  
 [10] J. D. Carter, D. Henderson, and I. Butterfield, A comparison of frequency downshift models of wave trains on deep water, *Phys. Fluids* **31**, 013103 (2019).  
 [11] H. N. Chan, R. H. J. Grimshaw, and K. W. Chow, Modeling internal rogue waves in a long wave-short wave resonance framework, *Phys. Rev. Fluids* **3**, 124801 (2018).  
 [12] K. Dysthe, H. E. Krogstad, and P. Müller, Oceanic rogue waves, *Annu. Rev. Fluid Mech.* **40**, 287 (2008).  
 [13] C. Kharif, E. Pelinovsky, and A. Slunyaev, *Rogue waves in the ocean* (Springer-Verlag, Berlin/Heidelberg, 2009).

- [14] M. Onorato, S. Residori, U. Bortolozzo, A. Montina, and F. T. Arecchi, Rogue waves and their generating mechanisms in different physical contexts, *Phys. Rep.* **528**, 47 (2013).
- [15] A. Toffoli, T. Waseda, H. Houtani, T. Kinoshita, K. Collins, D. Proment, and M. Onorato, Excitation of rogue waves in a variable medium: An experimental study on the interaction of water waves and currents, *Phys. Rev. E* **87**, 051201(R) (2013).
- [16] A. Toffoli, L. Fernandez, J. Monbaliu, M. Benoit, E. Gagnaire-Renou, J. M. Lefèvre, L. Cavaleri, D. Proment, C. Pakozdi, C. T. Stansberg, T. Waseda, and M. Onorato, Experimental evidence of the modulation of a plane wave to oblique perturbations and generation of rogue waves in finite water depth, *Phys. Fluids* **25**, 091701 (2013).
- [17] A. Cazaubiel, G. Michel, S. Lepot, B. Semin, S. Aumaitre, M. Berhanu, F. Bonnefoy, and E. Falcon, Coexistence of solitons and extreme events in deep water surface waves, *Phys. Rev. Fluids* **3**, 114802 (2018).
- [18] G. Dong, B. Liao, Y. Ma, and M. Perlin, Experimental investigation of the Peregrine Breather of gravity waves on finite water depth, *Phys. Rev. Fluids* **3**, 064801 (2018).
- [19] F. Baronio, S. Chen, P. Grelu, S. Wabnitz, and M. Conforti, Baseband modulation instability as the origin of rogue waves, *Phys. Rev. A* **91**, 033804 (2015).
- [20] H. N. Chan and K. W. Chow, Rogue waves for an alternative system of coupled Hirota equations: Structural robustness and modulation instabilities, *Stud. Appl. Math.* **139**, 78 (2017).
- [21] G. Zhang, Z. Yan, and X.-Y. Wen, Three-wave resonant interactions: Multi-dark-dark-dark solitons, breathers, rogue waves, and their interactions and dynamics, *Physica D* **366**, 27 (2018).
- [22] C. S. Willett, R. R. Leben, and M. F. Lavin, Eddies and tropical instability waves in the eastern tropical Pacific: A review, *Prog. Oceanogr.* **69**, 218 (2006).
- [23] J. N. Moum, M. J. McPhaden, D. Hebert, H. Peters, C. A. Paulson, and D. R. Caldwell, Internal waves, dynamic instabilities, and turbulence in the equatorial thermocline—An introduction, *J. Phys. Oceanogr.* **22**, 1357 (1992).
- [24] D. I Pullin and R. H. J. Grimshaw, Interfacial progressive gravity waves in a two-layer shear flow, *Phys. Fluids* **26**, 1731 (1983).
- [25] M. Ehmstroem and G. Villari, Linear water waves with vorticity: Rotational features and particle paths, *J. Diff. Eq.* **244**, 1888 (2008).
- [26] K. A. Belibassakis, B. Simon, J. Touboul, and V. Rey, A coupled-mode model for water wave scattering by vertically sheared currents in variable bathymetry regions, *Wave Motion* **74**, 73 (2017).
- [27] B. L. Segal, D. Moldabayev, H. Kalisch, and B. Deconinck, Explicit solutions for a long-wave model with constant vorticity, *Eur. J. Mech. B Fluids* **65**, 247 (2017).
- [28] A. Senthilkumar and H. Kalisch, Wave breaking in the KdV equation on a flow with constant vorticity, *Eur. J. Mech. B Fluids* **73**, 48 (2019).
- [29] R. Thomas, C. Kharif, and M. Manna, A nonlinear Schrödinger equation for water waves on finite depth with constant vorticity, *Phys. Fluids* **24**, 127102 (2012).
- [30] B. Liao, G. Dong, Y. Ma, and J. L. Gao, Linear-shear-current modified Schrödinger equation for gravity waves in finite water depth, *Phys. Rev. E* **96**, 043111 (2017).
- [31] A. T. da Silva and D. Peregrine, Steep, steady surface waves on water of finite depth with constant vorticity, *J. Fluid Mech.* **195**, 281 (1988).
- [32] C. W. Curtis, J. D. Carter, and H. Kalisch, Particle paths in nonlinear Schrödinger models in the presence of linear shear currents, *J. Fluid Mech.* **855**, 322 (2018).
- [33] K. L. Oliveras and C. W. Curtis, Nonlinear travelling internal waves with piecewise-linear shear profiles, *J. Fluid Mech.* **856**, 984 (2018).
- [34] H. C. Hsu, C. Kharif, M. Abid, and Y. Y. Chen, A nonlinear Schrödinger equation for gravity-capillary water waves on arbitrary depth with constant vorticity. Part 1, *J. Fluid Mech.* **854**, 146 (2018).
- [35] M. Francius and C. Kharif, Two-dimensional stability of finite-amplitude gravity waves on water of finite depth with constant vorticity, *J. Fluid Mech.* **830**, 631 (2017).
- [36] A. Abrashkin and E. Pelinovsky, Lagrange form of the nonlinear Schrödinger equation for low-vorticity waves in deep water, *Nonlin. Processes Geophys.* **24**, 255, (2017).
- [37] R. S. Johnson, On the modulation of water waves on shear flows, *Proc. Roy. Soc. A* **347**, 537 (1976).

- [38] M. Oikawa, K. Chow, and D. J. Benney, The propagation of nonlinear wave packets in a shear flow with a free surface, *Stud. Appl. Math.* **76**, 69 (1987).
- [39] S. A. Ellingsen and Y. Li, Approximate dispersion relations for waves on arbitrary shear flows, *J. Geophys. Res. Oceans* **122**, 9889 (2017).
- [40] H. N. Chan, B. A. Malomed, K. W. Chow, and E. Ding, Rogue waves for a system of coupled derivative nonlinear Schrödinger equations, *Phys. Rev. E* **93**, 012217 (2016).
- [41] A. Calini and C. M. Schober, Dynamical criteria for rogue waves in nonlinear Schrödinger models, *Nonlinearity* **25**, R99 (2012).
- [42] B. Kibler, A. Chabchoub, A. Gelash, N. Akhmediev, and V. E. Zakharov, Superregular Breathers in Optics and Hydrodynamics: Omnipresent Modulation Instability Beyond Simple Periodicity, *Phys. Rev. X* **5**, 041026 (2015).
- [43] R. H. J. Grimshaw and A. Tovbis, Rogue waves: Analytical predictions, *Proc. R. Soc. A* **469**, 20130094 (2013).
- [44] G. Mu, Z. Qin, K. W. Chow, and B. K. Ee, Localized modes of the Hirota equation:  $M$ th order rogue wave and a separation of variable technique, *Commun. Nonlinear Sci. Numer. Simul.* **39**, 118 (2016).
- [45] A. Ankiewicz, J. M. Soto-Crespo, and N. Akhmediev, Rogue waves and rational solutions of the Hirota equation, *Phys. Rev. E* **81**, 046602 (2010).
- [46] A. Constantin, The flow beneath a periodic travelling surface water wave, *J. Phys. A* **48**, 143001 (2015).
- [47] B. Deconinck, K. L. Oliveras, and V. Vasan, Relating the bottom pressure and the surface elevation in the water wave problem, *J. Nonlinear Math. Phys.* **19**, 179 (2012).
- [48] H. Borluk and H. Kalisch, Particle dynamics in the KdV approximation, *Wave Motion* **49**, 691 (2012).
- [49] R. S. Johnson, Models for the formation of a critical layer in water wave propagation, *Philos. Trans. R. Soc. A* **370**, 1638 (2012).
- [50] R. Grimshaw, Modulation of an internal gravity wave packet in a stratified shear flow, *Wave Motion* **3**, 81 (1981).